Gravitational waves by compact stars orbiting around rotating supermassive black holes

Masaru Shibata
Department of Earth and Space Science, Faculty of Science, Osaka University, Toyonaka, Osaka 560, Japan
(Received 19 July 1994)

To investigate the orbital evolution of compact stars moving around a supermassive black hole (SMBH) we have calculated the energy and angular momentum fluxes of gravitational waves induced by a test particle of mass μ orbiting on the equatorial plane of a rotating black hole of mass $M \gg \mu$ with eccentric orbits. First we analytically derive the post-Newtonian (PN) formula of the energy flux, and then, to see the relativistic effects correctly, we perform numerical calculations of the perturbation around a Kerr black hole. It is found that for highly relativistic orbits, the PN formula underestimates the energy fluxes by a factor $\lesssim 10$. We have also found that, in the case of highly relativistic and highly eccentric orbits, due to the spin (a) of the black hole, the energy flux changes by a factor of $\sim 10a/M$. Hence the orbital evolution of a compact star in the vicinity of a SMBH, which will exist in galactic nuclei, is largely affected by the spin angular momentum of the SMBH as well as other relativistic effects. The detection rate of gravitational waves from a SMBH by means of the proposed laser interferometric gravitational wave detector in space, such as LISA, also depends on these relativistic effects. A possibility of extracting the parameters of the SMBH from a signal of gravitational waves is also considered.

PACS number(s): 04.30.Db, 04.25.Nx, 97.60.Lf

I. INTRODUCTION

Gravitational waves induced by compact stars orbiting very closely around or plunging in a supermassive black hole (SMBH) of mass $10^6 - 10^9 M_\odot$, which will exist in galactic nuclei [1], are the most promising candidates of low frequency gravitational waves with a frequency of 10^{-5} to 10^{-1} Hz [2,3]. Such gravitational waves have a wide variety of information of galactic nuclei, such as the mass and spin of the SMBH, the characteristic orbit of the star, and so on. Thus the detection of gravitational waves has a possibility of seeing galactic nuclei.

Recently, the laser interferometric gravitational wave detector in space, such as the Laser Interferometer Space Antenna (LISA), has been proposed [4]. Such a detector has the ability to detect gravitational waves of amplitude $h \sim 10^{-20} - 10^{-21}$ for burst sources with a frequency $f \sim 10^{-1}$–10^{-4} Hz and $h \sim 10^{-23}$ for periodic sources with $f \sim 10^{-1}$–10^{-3} Hz for one year integration [4,5]. If a compact star, such as black hole, neutron star, or white dwarf, orbits around a SMBH of $10^6 M_\odot$ circularly, it does not suffer the tidal disruption and emits gravitational waves of the amplitude and frequency

$$h \sim 10^{-23}\left(\frac{1\ \mathrm{Gpc}}{R}\right)\left(\frac{\mu}{1M_\odot}\right)\left(\frac{5M}{r}\right),$$
$$f \sim \frac{1}{\pi}\sqrt{\frac{M}{r^3}} = (6\times 10^{-3}\ \mathrm{Hz})\left(\frac{10^6 M_\odot}{M}\right)\left(\frac{5M}{r}\right)^{3/2}, \tag{1.1}$$

where R, r, M, and μ are the distances from the SMBH to Earth, the orbital radius of the compact star, the mass of the SMBH, and the mass of the compact star, respectively. Also, if a compact object plunges into a SMBH, the amplitude and frequency will become [6]

$$h \sim 10^{-21}\left(\frac{10\ \mathrm{Mpc}}{R}\right)\left(\frac{\mu}{1M_\odot}\right),$$
$$f \sim \frac{0.4}{2\pi}\frac{1}{M} = (1.3\times 10^{-2}\mathrm{Hz})\left(\frac{10^6 M_\odot}{M}\right). \tag{1.2}$$

Hence, the burst gravitational waves which are radiated when a compact star plunges into a SMBH within ~ 10 Mpc or the periodic gravitational waves which are emitted by a compact object with an eccentric orbit around a SMBH within 1 Gpc, will be detected by LISA. The subject of the present paper is about the features of such gravitational waves.

Compact stars as well as normal stars are consumed into the galactic nuclei due to the two-body relaxation process, in particular, due to the loss cone effect [7,8]: In the system of a star cluster around a SMBH, the stars are scattered by the many two-body encounters. There, their angular momentums are exchanged and in some cases they reduce to less than $J_{\min}$, which is the minimum angular momentum of the star around the SMBH (i.e., below $J_{\min}$, the star is removed from the system due to the tidal disruption and/or plunge into the SMBH). The rate of the consumption in the normal galaxy has been estimated [8] as

$$F \sim \pi n_{\rm ac}(J_{\rm min}/v)^2 v \sim \pi r_t r_{\rm ac} n_{\rm ac} v$$
$$\sim 3\times 10^{-6}\left(\frac{M}{10^6 M_\odot}\right)\left(\frac{r_t}{10M}\right)\left(\frac{r_{\rm ac}}{0.1\ {\rm pc}}\right)\left(\frac{n_{\rm ac}}{10^5\ {\rm pc}^{-3}}\right)\left(\frac{v}{200\ {\rm km/s}}\right)\ {\rm yr}^{-1}, \tag{1.3}$$

where v, r_t, $r_{\rm ac}$, and $n_{\rm ac}$ denote the rms velocity of the stars in the isothermal core, the consumption radius $J_{\rm min}^2/M$ inside which the star is consumed, the accretion radius $\sim M/v^2$, and stellar density at $r_{\rm ac}$, respectively. The regions for $r\langle r_{\rm ac}$ and $r\rangle r_{\rm ac}$ are often called the stellar cusp and the isothermal core [8], respectively. Since only ~ 10 galaxies exist within 10 Mpc, the burst gravitational waves emitted by the star plunging into the SMBH will not be detected frequently. (But, M87 may be a strong burst source [2].) On the other hand, gravitational waves by a star with a highly eccentric orbit around a SMBH supplied in the case that the star reduces its angular momentum to $J \gtrsim J_{\rm min}$ and it escapes the tidal disruption (i.e., the star is a compact object) may be detected frequently because the event rate seems to be significant. Let us consider the evolution of such a star in the galactic nuclei.

According to the theory of stellar consumption [7] in normal galactic nuclei, the consumption rate is determined by the physical feature of the star cluster around $r_{\rm crit} \sim 1$–10 pc. Here, $r_{\rm crit}$ is defined as a radius at which the change rate of the angular momentum j during one orbital period equals $J_{\rm min}$. That is [7],

$$j \equiv J_{\rm crit}\left(\frac{t_d}{t_r}\right)^{1/2} \simeq (Mr_{\rm crit})^{1/2}\left(\frac{2\pi(r_{\rm crit}^3/M)^{1/2}}{t_r}\right)^{1/2} = J_{\rm min},$$

where t_d and t_r are the dynamical time scale of a star at $r_{\rm crit}$ and the relaxation time scale of the clusters [8], respectively. Thus, we consider the evolution of stars around $r_{\rm crit}$. If a star around $r_{\rm crit}$ happens to reduce its angular momentum to $J \gtrsim J_{\rm min}$, the star comes to a highly eccentric orbit, $e \sim 1$. Such a star passes very close to the SMBH and loses the energy and angular momentum by means of gravitational radiation sufficiently. The time scales of the energy and angular momentum dissipations due to gravitational radiation for $e \sim 1$ orbits are crudely estimated by the quadrupole formula and, respectively, become

$$t_{\rm GWE} \equiv \frac{E}{dE/dt} \sim \frac{M\mu/2a_0}{(32/5)M^3\mu^2 a_0^2 (r_p r_a)^{-7/2}(1+73e^2/24+37e^4/96)}$$
$$\sim 4\times 10^4 yr\left(\frac{r_p}{4M}\right)^{7/2}\left(\frac{r_a}{10\ {\rm pc}}\right)^{1/2}\left(\frac{M}{10^6 M_\odot}\right)^{1/2}\left(\frac{M}{10^6\mu}\right) \tag{1.4}$$

and

$$t_{\rm GWJ} \equiv \frac{J}{dJ/dt} \sim \frac{\mu(2Mr_p)^{1/2}}{(32/5)M^{5/2}\mu^2 a_0^{1/2}(r_p r_a)^{-2}(1+7e^2/8)}$$
$$\sim 2\times 10^{12}{\rm yr}\left(\frac{r_p}{4M}\right)^{5/2}\left(\frac{r_a}{10\ {\rm pc}}\right)^{3/2}\left(\frac{10^6 M_\odot}{M}\right)^{1/2}\left(\frac{M}{10^6\mu}\right), \tag{1.5}$$

where μ, r_p, r_a are the mass of the star, periastron, apastron, respectively, and a_0 is the semimajor axis, $(r_p+r_a)/2$. On the other hand, the time scale of the two body encounter [7] is approximately

$$t_r \sim (2\times 10^{10}\ {\rm yr})\left(\frac{v}{200\ {\rm km/s}}\right)^3\left(\frac{M_\odot}{\mu}\right)^2\left(\frac{\ln(10^6)}{\ln(N)}\right)\left(\frac{10^5\ {\rm pc}^{-3}}{n}\right), \tag{1.6}$$

for $r > r_{ac}$ and

$$\sim (2\times 10^{10}\ {\rm yr})\left(\frac{r}{r_{\rm ac}}\right)^{1/4}\left(\frac{10^6 M_\odot}{M}\right)^{1/2}\left(\frac{M}{10^6\mu}\right)^2\left(\frac{\ln(10^6)}{\ln(N)}\right)\left(\frac{r_{\rm ac}}{0.1\ {\rm pc}}\right)^{3/2}\left(\frac{10^2}{n_{\rm ac}r_{\rm ac}^3}\right), \tag{1.7}$$

for $r < r_{\rm ac}$. Here v, n, and N are the velocity dispersion, the number density, and the total number of stars, respectively. Also, we assume that the stellar density behaves as $\propto r^{-7/4}$ for $r < r_{\rm ac}$ [7,8]. The above time scales mean that energy is lost by gravitational radiation on a time scale much faster than the relaxation time scale, while angular momentum is not lost by gravitational radiation as fast; only in the case r_a is it small enough

(if $M = 10^6 M_\odot$, $r_a \lesssim 0.5$ pc), $t_{\rm GWJ} < t_r$. Hence, the evolution of the star is affected by the two-body scattering before the orbit shrinks sufficiently. In such a case, we cannot expect the rigid capture rate of stars because their eccentric orbits will be changed to the noneccentric orbits by the two-body encounters. However, we can expect a rigid capture rate for the following reason. The energy dissipation during a round trip near the SMBH is approximately

$$\Delta E \equiv \frac{dE}{dt} t_p \sim 25 \frac{M\mu}{r_a} \left(\frac{10^6 \mu}{M}\right) \left(\frac{4M}{r_p}\right)^{7/2} \times \left(\frac{r_a}{10\ {\rm pc}}\right) \left(\frac{10^6 M_\odot}{M}\right), \tag{1.8}$$

where we define t_p as $2\pi (a_0^3/M)^{1/2}$. This equation means that once the star passes in the vicinity of the SMBH, $r_p \sim 4M$, it loses its energy much larger than the original one. For $M = 10^6 M_\odot$, even if the apastron of the star is initially at 10 pc, it changes to ~ 0.4 pc after one orbital period. Then $t_{\rm GWJ}$ becomes $\lesssim t_r$, so that the effects of the two-body process to the orbital evolution become weak and subsequent orbital evolutions are determined by the emission of gravitational radiation. It should be noted that only in the case $r_p \sim 4M$ is the sufficient energy dissipated by gravitational radiation. Hence, we may expect a rigid capture rate for compact stars, which is essentially the same as the consumption rate for $r_t \sim r_p \sim 4M$. The capture rate of a compact star with a high eccentricity is expected as

$$F_{\rm cap} \sim 3 \times 10^{-8} \epsilon \left(\frac{M}{10^6 M_\odot}\right) \left(\frac{r_p - r_{\rm MB}}{M}\right) \left(\frac{r_{\rm ac}}{0.1\ {\rm pc}}\right) \times \left(\frac{n_{\rm ac}}{10^5\ {\rm pc}^{-3}}\right) \left(\frac{v}{200\ {\rm km/s}}\right) {\rm yr}^{-1}, \tag{1.9}$$

where $r_{\rm MB}$ is the radius of the marginally bound orbit; i.e., inside $r_{\rm MB}$ the star with $E \sim 0$ must plunge into the SMBH. ϵ denotes a fraction of the compact stars in the cluster in units of 10%. ϵ is expected to be $\lesssim 1$ because the main sequence stars with $\mu \gtrsim 0.9 M_\odot$ have already become compact stars [9].

To evaluate the event rate of periodic sources, we must obtain the number of host galaxies and the duration time of a typical event. Extrapolating the number of the galaxies to the cosmological scale [10], there will exist about $N_g \sim 10^7$ galaxies within 1 Gpc. To accumulate sufficient phases of gravitational waves, the period of the compact star must be less than ~ 1 yr. If we impose that the period should be less than 10^{-4} yr to accumulate about 10^4 cycles of gravitational waves (i.e., effective signal $h_{\rm eff} \sim 10^2 h$ [2]), the condition becomes

$$r_a \lesssim 2 \times 10^{-6} \left(\frac{M}{10^6 M_\odot}\right)^{1/3} {\rm pc} = 40M \left(\frac{M}{10^6 M_\odot}\right)^{-2/3}. \tag{1.10}$$

From Eq. (1.4), we can calculate the duration time for such a star emitting gravitational waves with an amplitude high enough and it becomes

$$t_d \sim 20\ {\rm yr} \left(\frac{r_p}{4M}\right)^{7/2} \left(\frac{M}{10^6 M_\odot}\right)^{2/3} \left(\frac{M}{10^6 \mu}\right). \tag{1.11}$$

Gathering the above results, we may expect the event rate for a one-year search by LISA as

$$F_{\rm event} = F_{\rm cap} N_g \frac{t_d}{1\ {\rm yr}} \sim 6\epsilon \left(\frac{M}{10^6 M_\odot}\right)^{5/3} \left(\frac{M}{10^6 \mu}\right) \times \left(\frac{r_p}{4M}\right)^{7/2} \left(\frac{r_p - r_{\rm MB}}{M}\right) \left(\frac{r_{\rm ac}}{0.1\ {\rm pc}}\right) \times \left(\frac{v}{200\ {\rm km/s}}\right) \left(\frac{N_g}{10^7}\right) \left(\frac{n_{\rm ac}}{10^5\ {\rm pc}^{-3}}\right) {\rm yr}^{-1}. \tag{1.12}$$

Therefore, a few events per year may be expected.

From the above arguments, we can find that the emission of gravitational waves in the vicinity of the SMBH, i.e., highly relativistic region, plays several important roles. (1) The number of stars captured by the SMBH (i.e., $t_{\rm GWJ} < t_r$), which initially have a high eccentricity in the vicinity of $r_{\rm crit}$, are determined by the time scale of the angular momentum dissipation [Eq. (1.5)] as well as the energy dissipation of gravitational waves [Eq. (1.7)]. In particular, the energy flux is important because it determines the upper limit of r_p which corresponds to r_t in this situation, and the event rate is proportional to $(r_p - r_{mb}) r_p^{7/2}$. (2) The duration time in which a star keeps an eccentric orbit in the vicinity of a SMBH before it plunges into the SMBH is also determined by the energy flux of gravitational waves [Eq. (1.11)]. Hence, to obtain the event rate strictly, i.e., to calculate the orbital evolution of a compact star around a SMBH, we need the general relativistic formula of the energy and angular momentum fluxes. The purpose of the present paper is to evaluate these quantities correctly. Thus, the rest of the paper is organized as follows. In Sec. II, we derive the post-Newtonian (PN) formula of the energy flux induced by a particle orbiting on the equatorial plane of a spinning massive body and indicate the importance of the spin effect of the massive body. To see the spin effects as well as the relativistic fluxes of gravitational waves correctly, in Sec. III we perform the perturbation study around a Kerr black hole and calculate the energy and angular momentum fluxes. To see the possibility of extracting various parameters from a signal of gravitational waves, we also consider the Fourier spectrum of gravitational waves. Section IV gives the discussion.

Throughout this paper, we use the units of $c = G = 1$ and $M_\odot$ denotes the solar mass.

II. POST-NEWTONIAN FORMULA OF THE ENERGY FLUX

In this section, we analytically derive the energy flux of gravitational waves induced by a test particle of mass

μ orbiting around a rotating body of spin S and mass $M \gg \mu$ by the PN analysis. Throughout this paper, we fix the orbital plane of a test particle perpendicular to the spin axis (i.e., if we determine that the spin axis is parallel to the z axis, $\theta = \pi/2$). Of course, there is no physical reason why the test particle stays on the equatorial plane, and to see the orbital evolution of the particle around a Kerr black hole we should take into account general orbits. However in the case in which the particle has both an eccentricity and an orbital inclination with respect to the equatorial plane, the motion of the test particle becomes nonperiodic. We do not know how to evalute the energy flux of the gravitational waves locally in time and only in the averaged sense can we evaluate it. Therefore, to evaluate the energy flux of gravitational waves in the case that the test particle moves with a nonperiodic motion, we must integrate the orbit for the infinite time interval. Fortunately, the spin effects to the energy flux become maximum when the particle moves on the equatorial plane because the spin coupling terms appear in the form of $\mathbf{S} \cdot \mathbf{L}$ [11]. Hence, this is a good example to see the spin effects to the orbital evolution. For that reason, in this paper, we only consider the case in which the particle stays on the equatorial plane as a first step.

In the following, we treat the PN terms up to (post) $^{3/2}$-Newtonian ($P^{3/2}N$) order, i.e., up to the linear order in S. If higher terms in S appears in the equation of motion, we will neglect them. Since the first PN terms are treated previously [12,13], we here consider $N + P^{3/2}N$ equation of motion. Since $M \gg \mu$ is assumed, we set $\mu/M = 0$ in the equation of motion. Then the equation of motion [11] becomes

$$\frac{d^2r}{dt^2} = r\left(\frac{d\varphi}{dt}\right)^2 - \frac{M}{r^2} + \frac{2S}{r^2}\frac{d\varphi}{dt}, \tag{2.1}$$

$$r\frac{d^2\varphi}{dt^2} + 2\frac{d\varphi}{dt}\frac{dr}{dt} = -\frac{2S}{r^3}\frac{dr}{dt}. \tag{2.2}$$

Equation (2.2) can be integrated immediately as

$$r^2\frac{d\varphi}{dt} - \frac{2S}{r} = \frac{\hat{L}_z}{\mu} = \text{const} \equiv L_z, \tag{2.3}$$

where $\hat{L}_z$ is regarded as the z component of the angular momentum of the test particle. Subsituting Eq. (2.3) into Eq. (2.1), Eq. (2.1) can be also integrated as

$$\frac{1}{2}\left(\frac{dr}{dt}\right)^2 + \frac{L_z^2}{2r^2} + \frac{2SL_z}{r^3} - \frac{M}{r} = \frac{\hat{E}}{\mu} = \text{const} \equiv E, \tag{2.4}$$

where $\hat{E}$ is the total energy of the system.

To obtain an orbital motion of a test particle, we must solve Eq. (2.4), in which, however, the elliptical integral appears if we try to solve Eq. (2.4) itself. To avoid treating such a complicated function, we use a technique developed by Damour and Deruelle [14]. First, we change the radial variable as

$$\bar{r} = r - \frac{2S}{L_z}. \tag{2.5}$$

Then Eq. (2.4) becomes

$$\frac{1}{2}\left(\frac{d\bar{r}}{dt}\right)^2 + \frac{\beta}{2\bar{r}^2} + \frac{M}{\bar{r}} = E, \tag{2.6}$$

where $\beta = L_z^2 + 4SM/L_z$. In Eq. (2.6), we have ignored the terms of $O(S^n)$, $n \geq 2$, because we only consider the linear terms in S. Since Eq. (2.6) is the same form as that of the Kepler problem, the solution is obtained immediately as

$$\bar{r} = \frac{M}{2|E|} - q\cos u, \tag{2.7}$$

$$t = \frac{1}{\sqrt{2|E|}}\left(\frac{M}{2|E|}u - q\sin u\right), \tag{2.8}$$

where $q^2 = M^2/4E^2 - \beta/2|E|$, and u is an eccentric anomaly [15] which covers the interval 0 to 2π. The periastron r_p and apastron r_a become

$$\begin{aligned} r_p &\simeq \frac{M}{2|E|} - \sqrt{\frac{M^2}{4E^2} - \frac{L_z^2}{2|E|}} \\ &\quad + \frac{2S}{L_z}\left(1 + \frac{M}{\sqrt{M^2 - 2|E|L_z^2}}\right), \\ r_a &\simeq \frac{M}{2|E|} + \sqrt{\frac{M^2}{4E^2} - \frac{L_z^2}{2|E|}} \\ &\quad + \frac{2S}{L_z}\left(1 - \frac{M}{\sqrt{M_2 - 2|E|L_z^2}}\right). \end{aligned} \tag{2.9}$$

Hence if the energy and angular momentum of the test particle are the same, the periastron for $S < 0$ (retrograde orbit) is always smaller than that for $S > 0$ (prograde orbit) and the apastron for $S < 0$ is larger than that for $S > 0$.

Using u as an independent variable, Eq. (2.3) becomes

$$\frac{d\varphi}{du} = \frac{L_z}{\sqrt{2|E|}}\frac{\bar{r}}{r^2}\left(1 + \frac{2S}{rL_z}\right). \tag{2.10}$$

To solve Eq. (2.10), we use the same technique described before. We change the radial variable as

$$r = \tilde{r} + \frac{S}{L_z}. \tag{2.11}$$

Then Eq. (2.10) becomes

$$\frac{d\varphi}{du} = \frac{L_z}{\sqrt{2|E|}}\frac{\bar{r}}{\bar{r}^2}. \tag{2.12}$$

We introduce the parameters

$$\frac{M}{2|E|}=a_0,\quad \frac{M}{2|E|}+\frac{S}{L_z}=a',\quad \frac{q}{a}=e,\quad \frac{q}{a'}=e'. \tag{2.13}$$

Then Eq. (2.12) becomes

$$\frac{d\varphi}{du}=\frac{L_z a_0}{\sqrt{2|E|}a'^2}\frac{1-e\cos u}{(1-e'\cos u)^2}. \tag{2.14}$$

Since the relation

$$(1-e\cos u)(1-e_s\cos u)=(1-e'\cos u)^2+O(S^2), \tag{2.15}$$

where $e_s=2e'-e$, holds, Eq. (2.14) becomes the familiar form

$$\frac{d\varphi}{du}=\frac{L_z a_0}{\sqrt{2|E|}a'^2}\frac{1}{1-e_s\cos u}. \tag{2.16}$$

The solution of Eq. (2.16) is

$$\varphi=\frac{2L_z a_0}{\sqrt{2|E|(1-e_s^2)}a'^2}\arctan\left(\sqrt{\frac{1+e_s}{1-e_s}}\tan\frac{u}{2}\right). \tag{2.17}$$

Here let us consider a trajectory of a test particle. When the particle moves from the apastron to the apastron, u changes $-\pi\to\pi$ and φ changes

$$-\frac{\pi L_z a_0}{\sqrt{2|E|(1-e_s^2)}a'^2}\to\frac{\pi L_z a_0}{\sqrt{2|E|(1-e_s^2)}a'^2}. \tag{2.18}$$

Hence the charge ($\Delta\varphi$) in φ during one orbit is

$$\Delta\varphi=\frac{2\pi L_z a_0}{\sqrt{2|E|(1-e_s^2)}a'^2}=2\pi(1-\delta)+O(S^2), \tag{2.19}$$

where $\delta=4MS/L_z^3$. Equation (2.19) means that the spin-orbit coupling force causes the periastron shift, and in the case of the prograde (retrograde) orbits it is negative (positive). Eq. (2.17) is rewritten as

$$\tan\frac{\varphi'}{2}=\sqrt{\frac{1+e_s}{1-e_s}}\tan\frac{u}{2}, \tag{2.20}$$

where $\varphi'=\varphi(1+\delta)$ and moves 0 to 2π when u moves 0 to 2π. Then the relation between r and φ' becomes

$$r=a_s\frac{1-e_s^2}{1+e_s\cos\varphi'}, \tag{2.21}$$

where

$$a_s=\frac{M}{2|E|}+\frac{2S}{L_z}, \tag{2.22}$$

and the explicit form of e_s is

$$e_s=\left(1-\frac{2|E|L_z^2}{M^2}-\frac{16S|E|}{ML_z}+\frac{16SE^2L_z}{M^3}\right)^{1/2}. \tag{2.23}$$

Next, we consider the energy flux. The general PN formula of the energy flux from a spinning binary was derived by Kidder *et al.* [11]. In the present case, it becomes

$$\frac{dE}{dt}=\frac{8}{15}\left[\frac{12v^2}{r^4}-\frac{11}{r^4}\left(\frac{dr}{dt}\right)^2+\frac{S}{Mr^4}\frac{d\varphi}{dt}\left\{27\left(\frac{dr}{dt}\right)^2-37v^2-\frac{12M}{r}\right\}\right]. \tag{2.24}$$

We define the averaged energy flux which is just the physically meaningful quantity, i.e., gauge invariant quantity, as

$$\left\langle\frac{dE}{dt}\right\rangle=\frac{1}{T}\int_0^T dt\frac{dE}{dt}, \tag{2.25}$$

where $T=2\pi M/(2|E|)^{3/2}$ is the orbital period. Since the relations

$$v^2=2\left(E+\frac{M}{r}\right),\qquad \left(\frac{dr}{dt}\right)^2=2\left(E+\frac{M}{r}-\frac{2SL_z}{r^3}-\frac{L_z^2}{2r^2}\right) \tag{2.26}$$

hold, the averaged energy flux becomes

$$\left\langle\frac{dE}{dt}\right\rangle=\frac{8M^2}{15T}\int_0^T dt\left(\frac{2E}{r^4}+\frac{2M}{r^5}+\frac{11L_z^2}{r^6}-\frac{20ESL_z}{Mr^6}+\frac{12SL_z}{r^7}-\frac{27SL_z^3}{Mr^8}\right). \tag{2.27}$$

Hence all we have to do is evaluate

$$\frac{1}{T}\int_0^T dt r^{-n}\quad\text{for } 4\le n\le 8. \tag{2.28}$$

Using the equation $dt=d\varphi' r^2(1-\delta)(L_z-2S/r)$, the average of r^{-n} becomes

$$\langle r^{-n}\rangle=\frac{2\pi(1-\delta)}{L_z T}\left\{\frac{1}{a_s(1-e_s^2)}\right\}^{n-2}\times\left\{I_{n-2}-\frac{2S}{L_z a_s(1-e_s^2)}I_{n-1}\right\}, \tag{2.29}$$

where

$$I_n=\int_0^{2\pi}d\varphi(1+e_s\cos\varphi)^n. \tag{2.30}$$

After straightforward calculations, we obtain the averaged energy flux as

$$\left\langle \frac{dE}{dt} \right\rangle = \frac{32M^3\mu^2}{5}\frac{Q^5}{(1-e_s^2)^{7/2}}\left\{1+\frac{73}{24}e_s^2+\frac{37}{96}e_s^4 - \frac{MS}{123L_z^3}\left(193+\frac{1313}{2}e_s^2+\frac{297}{8}e_s^4-\frac{249}{16}e_s^6\right)\right\}, \tag{2.31}$$

where $Q = 2|E|/M$ and can be written as

$$Q \simeq \frac{1}{a_s}\left(1+\frac{2S}{L_z a_s}\right). \tag{2.32}$$

Using Eq. (2.32), Eq. (2.31) is rewritten as

$$\left\langle \frac{dE}{dt} \right\rangle = \frac{32M^3\mu^2}{5}\frac{1}{a_s^5(1-e_s^2)^{7/2}}\left\{1+\frac{73}{24}e_s^2+\frac{37}{96}e_s^4 - \frac{MS}{12L_z^3}\left(73+\frac{823}{2}e_s^2-\frac{2253}{8}e_s^4-\frac{989}{16}e_s^6\right)\right\}. \tag{2.33}$$

The first line of Eq. (2.33) was previously obtained by Peters and Mathews [16], and, in the case $e_s = 0$, Eq. (2.33) reduces to the formula derived by Kidder *et al* [11].

Since $L_z \sim (2Mr_p)^{1/2} \propto \{a_s(1-e_s)\}^{1/2}$, the spin terms become large when the orbit becomes highly eccentric. Let us discuss the effects of the spin terms fixing the energy and angular momentum as $E \sim 0, r_p \sim 4M$, $e_s \sim 1$, which corresponds to the most eccentric bound orbit in the Schwarzschild spacetime. In this case, the second terms of Eq. (2.32) become $\sim 8S/M^2$. Therefore, even if the energy and angular momentum of the test particle are the same, a large difference of the energy flux will occur depending on the spin of the black hole. This effect is also expected from the location of the periastron of the test particle orbiting around black holes with different spins. As shown above, the periastron of the test particle is smaller for $S < 0$ and, as shown in a previous paper [17], the energy flux induced by a particle with an eccentric orbit is almost determined by the periastron of the particle; for a smaller periastron, the energy flux becomes larger. Hence the energy flux for $S < 0$ becomes larger than that for $S > 0$ even if the energy and angular momentum of a test particle are the same.

This feature is important when we consider the event rate of gravitational waves from galactic nuclei. The reason is as follows: The event rate is determined by the amplitude of gravitational waves h, the duration time of the event, $E/\dot{E}$, and the sensitivity of a detector. The number of events which can be detected by a detector with a sensitivity is proportional to h^{-3}. Thus, the event rate is roughly proportional to $h^{-3}E/\dot{E}$. Where the test particle with $E \sim 0$ and $e_s \sim 1$ is concerned, the energy flux highly depends on the spin of the SMBH, so that the event rate will also depend on it.

The formula of the energy flux derived above may be used only for the large orbital radius of the test particle because it is derived under the PN approximation, i.e., $v \ll 1$. Thus, to investigate whether spin effects are large or not even in the case $v \lesssim 1$, we will perform the numerical calculation of the perturbation study around a Kerr black hole in the next section.

III. PERTURBATION STUDY AND NUMERICAL RESULTS

A. Basic equation

In this section, we perform numerical calculations of the perturbation study of gravitational waves induced by a particle of mass μ moving with an eccentric orbit around a Kerr black hole of mass M and spin parameter a. Basic formulas to perform the perturbation study around a Kerr black hole are described in previous papers [18–20,6], so we only describe points of the method. We use the Sasaki-Nakamura equation [20], which is transformed from the Teukolsky equation [21], and its radial wave equation is

$$\left[\frac{d^2}{dr^{*2}} - F(r)\frac{d}{dr^*} - U(r)\right]X_{lmw}(r) = S_{lmw}(r), \tag{3.1}$$

where r^* is a tortoise coordinate defined by $dr^*/dr = (r^2+a^2)/(r^2-2Mr+a^2)$ and potentials $F(r)$ and $U(r)$ are well-behaved functions at $r^* \to \pm\infty$. $S_{lmw}(r)$ is a source term in the case of an eccentric orbit it is nonvanishing only at $r \le r_a$, where r_a is the radius of the apastron. The solution of the radial wave function at infinity is obtained by the Green function method:

$$X_{lmw} = e^{iwr^*}\frac{c_0}{2iwA_{\rm in}}\int_{-\infty}^{r_a^*}\frac{SX_{\rm in}^{(0)}}{\gamma}dr^*, \tag{3.2}$$

where c_0 and γ are a complex constant and a function of r, respectively [14]. $X_{\rm in}^{(0)}$ is a homogeneous function of Eq. (3.1) with the boundary conditions

$$X_{\rm in}^{(0)} \to A_{\rm out}e^{iwr^*} + A_{\rm in}e^{-iwr^*}, \quad r^* \to \infty, \qquad X_{\rm in}^{(0)} \to e^{-ikr^*}, \quad r^* \to -\infty, \tag{3.3}$$

where $k = \omega - m(M-\sqrt{M^2-a^2})/(2Ma)$.

In the case of eccentric orbits, the angular frequency of gravitational waves becomes discrete [17] and is written as

$$\omega_n = \frac{m\Delta\varphi + 2\pi n}{\Delta t}, \quad n = 0, \pm1, \pm2, \ldots, \tag{3.4}$$

where Δt and $\Delta\varphi$ denote the orbital period and rotation angle during Δt, respectively. [i.e., $(\Delta\varphi - 2\pi)$ is the periastron shift.] Then, using $X_{lm\omega}$, the wave form at infinity, the energy and angular momentum fluxes are, respectively, written as

$$h_+ - ih_\times = \frac{16\pi}{R\Delta t}\sum_{n=-\infty}^{\infty}\sum_{l=2}^{\infty}\sum_{m=-l}^{l}\frac{X_{lm\omega_n}}{c_0}\frac{{}_{-2}S_{lm}^{a\omega_n}}{\sqrt{2\pi}}e^{i\omega_n(r^*-t)+im\varphi}, \tag{3.5}$$

$$\left\langle\frac{dE}{dt}\right\rangle = \frac{16\pi}{\Delta t^2}\sum_{n=-\infty}^{\infty}\sum_{l=2}^{\infty}\sum_{m=-l}^{l}\omega_n^2\left|\frac{X_{lmn}}{c_0}\right|^2, \tag{3.6}$$

$$\left\langle\frac{dJ_z}{dt}\right\rangle = \frac{16\pi}{\Delta t^2}\sum_{n=-\infty}^{\infty}\sum_{l-2}^{\infty}\sum_{m=-l}^{l}\omega_n m\left|\frac{X_{lmn}}{c_0}\right|^2, \tag{3.7}$$

where ${}_{-2}S_{lm}^{a\omega_n}$ is a spheroidal harmonics function. Note that to perform the sum in Eqs. (3.5)–(3.7), we can make use of symmetry relations as

$$\begin{aligned} {}_{-2}S_{l-m}^{a\omega_{-n}} &= {}_{-2}S_{lm}^{a\omega_n}, \\ \bar{X}_{l-m-n} &= X_{lmn}. \end{aligned} \tag{3.8}$$

The equations of motion of a test particle are

$$\begin{aligned} \frac{d\varphi}{d\tau} &= \frac{1}{r^2}\left[-(aE'-L_z)+\frac{a}{\Delta}\left\{E'(r^2+a^2)-aL_z\right\}\right], \\ \frac{dt}{d\tau} &= \frac{1}{r^2}\left[-(aE'-L_z)a\right. \\ &\quad \left.+\frac{a^2+r^2}{\Delta}\left\{E'(R^2+a^2)-aL_z\right\}\right], \\ \frac{dr}{d\tau} &= \pm\sqrt{V(r)}, \end{aligned} \tag{3.9}$$

where $\Delta = r^2 - 2Mr + a^2$ and

$$\begin{aligned} V(r) = &[\{E'(r^2+a^2)-aL_z\}^2 \\ &-\Delta\{(E'a-L_z)^2+r^2\}]r_{-4}. \end{aligned} \tag{3.10}$$

We consider the case in which there are three real roots for $V(r)=0$, $r_1 < r_2 < r_3$. Here, the periastron r_p and apastron r_a correspond to r_2 and r_3, respectively. Note that E' used in Eq. (3.9) is the energy of the test particle including the rest mass energy. Hence, E in Sec. II can be regarded as $E'-1$.

Since we consider bound orbits, E' must be less than $V_{\max}$, which is the local maximum of V between r_1 and r_2. In the case $E' = V_{\max} = 1$, L_z and r_p become $2M + 2\sqrt{M^2 - aM} \equiv L_{\rm MB}$ and $2M - a + 2\sqrt{M^2 - aM} \equiv r_{\rm MB}$, respectively, which is the so-called radius of marginally bound orbit (see also Fig. 1).

As for numerical methods to solve X_{lmn} and ${}_{-2}S_{lm}^{a\omega}$, we use the same methods as those described in [19], and omit them here. We describe only strategy of numerical calculations briefly. In the sum for l modes, we consider up to $l=6$ to save the computational time. This will not cause the large error because the contribution from $l \geq 7$ was at most $\leq 5\times10^{-5}$ for $r_p \geq 10M$ and $\sim 10^{-3}$ for $r_p \sim 5M$ in the case where a test particle moves with a circular orbit [18]. As for the sum for n modes, we let the numerical code compute the fluxes for n modes so as to obey the order such as $n = 0, 1, 2, \ldots$ and $n = -1, -2, \ldots$, and truncate the sum for higher $|n|$ modes if the following conditions are satisfied:

$$\begin{aligned} \left(\frac{dE}{dt}\right)_{n+1} &< 3\times10^{-6}\sum_{k=0}^{n}\left(\frac{dE}{dt}\right)_k \quad \text{for } n>0, \\ \left(\frac{dE}{dt}\right)_{m-1} &< 3\times10^{-6}\sum_{k=m}^{n}\left(\frac{dE}{dt}\right)_k \quad \text{for } m<0. \end{aligned} \tag{3.11}$$

To check the accuracy of the numerical code, we compare numerical results for $a=0$ with those previously calculated by us in the case of a Schwarzschild black hole [17], in which we claimed that relative error is less than 10^{-4}. It is found that the present results agree with them within the accuracy $\lesssim 2\times10^{-4}$. To check the accuracy of the numerical results for $a \neq 0$, we also compare our results for the limit of the circular orbit with previous results [18]. We also find that the accuracy is less than $\sim 10^{-4}$. Hence, we believe that the numerical error in total is at most $\sim 10^{-3}$ for $r_p \sim 5M$ and $\sim 10^{-4}$ for $r_p \geq 10M$.

B. The energy and angular momentum fluxes

To clarify orbital bounds, which a test particle can travel, first of all, we show the allowed regions of (E', L_z)

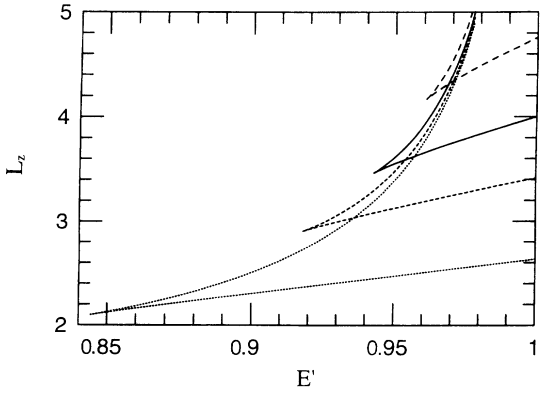

FIG. 1. The allowed region of E' and L_z for bound orbits of the test particle for $a/M = 0.9, 0.5, 0, -0.9$. The dotted, dashed, solid, and long dashed lines are for $a/M = 0.9, 0.5, 0, -0.9$, respectively. The vertical and horizontal lines denote L_z/M and E', respectively. In the figure, the upper line corresponds to the series of the circular orbit and another line corresponds to the series of the most eccentric orbit. The allowed region for a bound orbit is between two lines.

for bound orbits of the test particle for $a/M = 0.9, 0.5, 0, -0.9$ in Fig. 1. (Note that $a < 0$ means that the particle has a retrograde orbit around a black hole). In this figure, we describe two lines; the upper line corresponds to the series of the circular orbit (i.e., $e = 0$ or the minimum value of E' for a given L_z) and another line corresponds to the series of the most eccentric orbit (i.e., the maximum value of E' for a given L_z). That is, both lines are described by

$$E' = \frac{r^{3/2} - 2Mr^{1/2} + aM^{1/2}}{r^{3/4}(r^{3/2} - 3Mr^{1/2} + 2aM^{1/2})^{1/2}}, \tag{3.12}$$

$$L_z = \frac{M^{1/2}(r^2 - 2aM^{1/2}r^{1/2} + a^2)}{r^{3/4}(r^{3/2} - 3Mr^{1/2} + 2aM^{1/2})^{1/2}},$$

and the lower and upper lines, respectively, correspond to $r_{mb} \le r \le r_{ms}$ and $r_{ms} \le r$, where r_{ms} denotes the radius of the last stable circular orbit for a given a. The allowed region for a bound orbit is between two lines. Clearly we can see that the allowed region is wider for larger a. This is due to the repulsive nature of the spin-orbit coupling such as $\mathbf{S} \cdot \mathbf{L}$ [11].

We have calculated the energy and angular momentum fluxes for a variety of parameters a, E', L_z in the above allowed region. First, to see the relativistic effect, we compare the energy and angular momentum fluxes with those by the quadrupole formula as [16]

$$\left(\frac{dE}{dt}\right)_0 = \frac{32|2E|^5}{5}\left(\frac{\mu}{M}\right)^2\left(1 + \frac{73}{24}e^2 + \frac{37}{96}e^4\right) \times (1 - e^2)^{-7/2}, \tag{3.13}$$

$$\left(\frac{dJ_z}{dt}\right)_0 = \frac{32|2E|^{7/2}}{5}\left(\frac{\mu}{M}\right)^2 M\left(1 + \frac{7}{8}e^2\right)(1 - e^2)^{-2},$$

where $e^2 = 1 + 2L_z^2E/M^2$. In comparing the relativistic fluxes with those by the quadrupole formula, we must specify two parameters [17,22,23]. Here, we specify the energy $E = E' - 1$ and the angular momentum L_z as two parameters. This is in a sense a natural parametrization because E and L_z are the gauge independent quantities, and in the Newtonian limit, the relativistic formula will agree with the quadrupole formula using this parametrization. In Fig. 2(a) and 2(b), we show the relative errors

$$1 - \frac{(dE/dt)_0}{dE/dt},$$

$$1 - \frac{(dJ_z/dt)_0}{dJ_z/dt},$$

where dE/dt and dJ_z/dt denote the fluxes by numerical calculations. Open triangle, open square, and filled triangle denote the relative errors for $a/M = 0$, 0.9, -0.9, respectively. From Fig. 2, we can see that the quadrupole formula underestimates both the energy and angular momentum fluxes. It is also found that the underestimate is larger for $a < 0$ and for smaller r_p. In the case $a = 0$, the underestimate of the energy flux becomes more than a factor of 5 for $r_p \lesssim 10\,M$. Furthermore for case $a = -0.9\,M$, the underestimate of the energy flux becomes about a factor of 5 even for $r_p \lesssim 15\,M$.

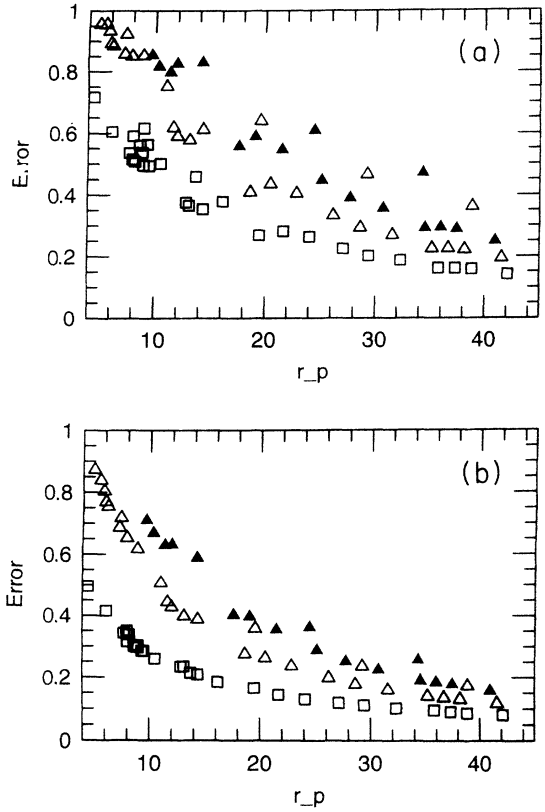

FIG. 2. Relative errors of (a) the energy and (b) the angular momentum fluxes defined as $1 - \dot{Q}_0/\dot{Q}$, where $\dot{Q}_0$ and $\dot{Q}$ are the flux by the quadrupole formula and the result by perturbative calculation, respectively. The horizontal line denotes r_p/M. Open square, open triangle, and filled triangle are for $a/M = 0.9$, 0, and -0.9, respectively.

As pointed out in a previous paper [17], these inconsistencies arise partly because in the quadrupole formula, we neglect the relativistic corrections, such as fast motion of the star and the scattering of gravitational waves by the curvature near the black hole. As another reason, we can mention the spin effect. To show that, in Fig. 3 we show the relative error of the energy flux using the formula Eq. (2.33) instead of the quadrupole formula. We can see that the relative errors become independent of the spin. This figure just indicates that the spin effect is important in the highly relativistic orbits. At this stage we may consider that the lowest order PN correction of the spin effect is taken into account and the error comes mainly from our ignorance of the PN correction except for the spin effect. To see that, in Fig. 4 we show the relative errors using the following formula instead of the quadrupole formula:

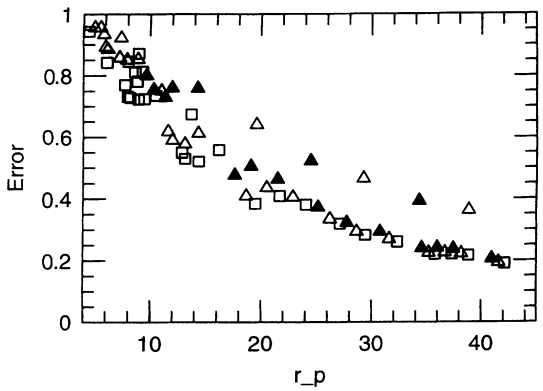

FIG. 3. Relative errors of the energy flux in the case where we use the $N + \mathrm{P}^{3/2}\mathrm{N}$ formula, i.e., Eq. (2.31) instead of the quadrupole formula.

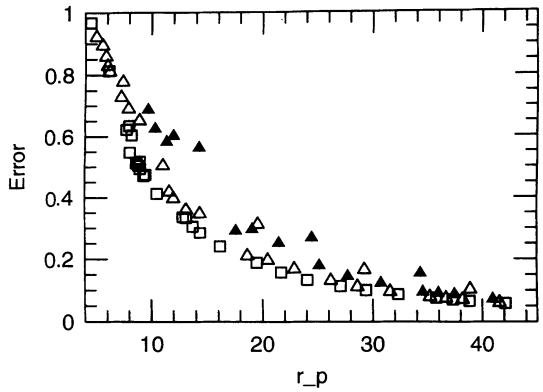

FIG. 4. Relative errors of the energy flux in the case where we use the $N + PN + \mathrm{P}^{3/2}\mathrm{N}$ formula, i.e., Eq. (3.14), instead of the quadrupole formula.

$$\frac{dE}{dt} = \frac{1024|E|^5}{5(1-e^2)^{7/2}}\left(\frac{\mu}{M}\right)^2\left\{\left(1+\frac{73}{24}e^2+\frac{37}{96}e^4\right) - \frac{MS}{12L_z^3}\left(193+\frac{1313}{2}e^2+\frac{297}{8}e^4-\frac{249}{16}e^6\right) + \frac{|E|}{168(1-e^2)}\left(13-6414e^2-\frac{27405}{4}e^4-\frac{5377}{16}e^6\right)\right\}, \tag{3.14}$$

where the last line is the first PN correction derived by Blanchet and Schäfer [13]. In this formula, $N + PN + P^{3/2}N$ terms except for the tail term [24] are taken into account. To put both the PN and $\mathrm{P}^{3/2}\mathrm{N}$ effects in the eccentricity, we define the eccentricity

$$e^2 \equiv 1 - \frac{2|E|L_z^2}{M^2} + 12|E| - 15E^2L_z^2 - \frac{16S|E|}{ML_z} + \frac{16SE^2L_z}{M^3}. \tag{3.15}$$

We should note that Eq. (3.15) reduces to the PN eccentricity derived by Blanchet and Schäfer [13] in the case $S = 0$. From Fig. 4, we can clearly see that the relative error becomes smaller than that in Fig. 3 irrespective of the spin; for $r_p \gtrsim 20\,M$, the error is less than $\sim 20\%$ and for $r_p \gtrsim 30\mathrm{M}$, the error is lest than $\sim 10\%$. However, even in this formula, the energy flux is underestimated by a factor of more than 2 for $r_p \lesssim 10\,M$, and the accuracy is not improved so much for $r_p \sim 5\,M$. It seems that this just indicates the limitation of the PN approximation for the emission problems of gravitational waves by a particle with a highly eccentric orbit. We need a more appropriate formula.

Next, let us investigate the spin effect minutely. To see the spin effect to the energy and angular momentum fluxes clearly, we compare dE/dt and dJ_z/dt for different spins, but with the same orbital parameters (E', L_z). In Fig. 5, we plot dE/dt and dJ_z/dt in a vertical axis and r_p in a horizontal axis. In Table I, we show the parameters adopted to write Fig. 5. From Fig. 5, it is found that the energy and the angular momentum fluxes behave as $\propto r_p^{-n}$, and indices are $n \sim 5$ and $n \sim 3$, respectively. To see the amplitude of gravitational waves, we show that for $a/M = 0.9$, 0 and $(E', L_z/M) = (0.9657447, 3.77964)$ as an example (Fig. 6). We can find the ratio of the maximum amplitude to be about 2/3. Since the ratio of the periastron is also 2/3, we may consider that the amplitude of gravitational waves behaves as $\propto r_p^{-1}$. On the other hand, the spin effect does not change the apastron so much, so the orbital period is not different because of the spin. Also, although the characteristic frequency of gravitational waves depends on the spin (see next subsection), the sensitivity of a broad-band detector to their frequencies is not different so much. Thus, we may say that the most important spin effect to the detection problem is to change the periastron of the test particle because the event rate depends only on the periastron, e.g., $h^{-3}E/\dot{E} \propto r_p^2$. This indicates that the spin effect to the event rate can be simply put in r_p in calculating the event rate approximately.

C. Spectrum of gravitational waves and extraction of parameters

In this subsection, we show Fourier spectrums of gravitational waves considering a possibility of extracting parameters of the source such as the eccentricity, the semi-major axis, the masses of the star and SMBH, and so on. Although an eccentric orbit of a star around a SMBH will evolve radiating gravitational waves, in the discussion below, we neglect the back reaction of gravitational waves. This is not an incorrect approximation for a SMBH of mass $\sim 10^6 M_\odot$ because the integration time by a detector ($\sim$ 1 yr) is short compared with the evolution time of the orbit, t_d.

Before we show the Fourier spectrums for highly relativistic orbits, we consider those for orbits in the Newtonian limit. The wave form of h_{ij} is written by the second derivative of the quadrupole moment. For example, the xx component h_{xx} is

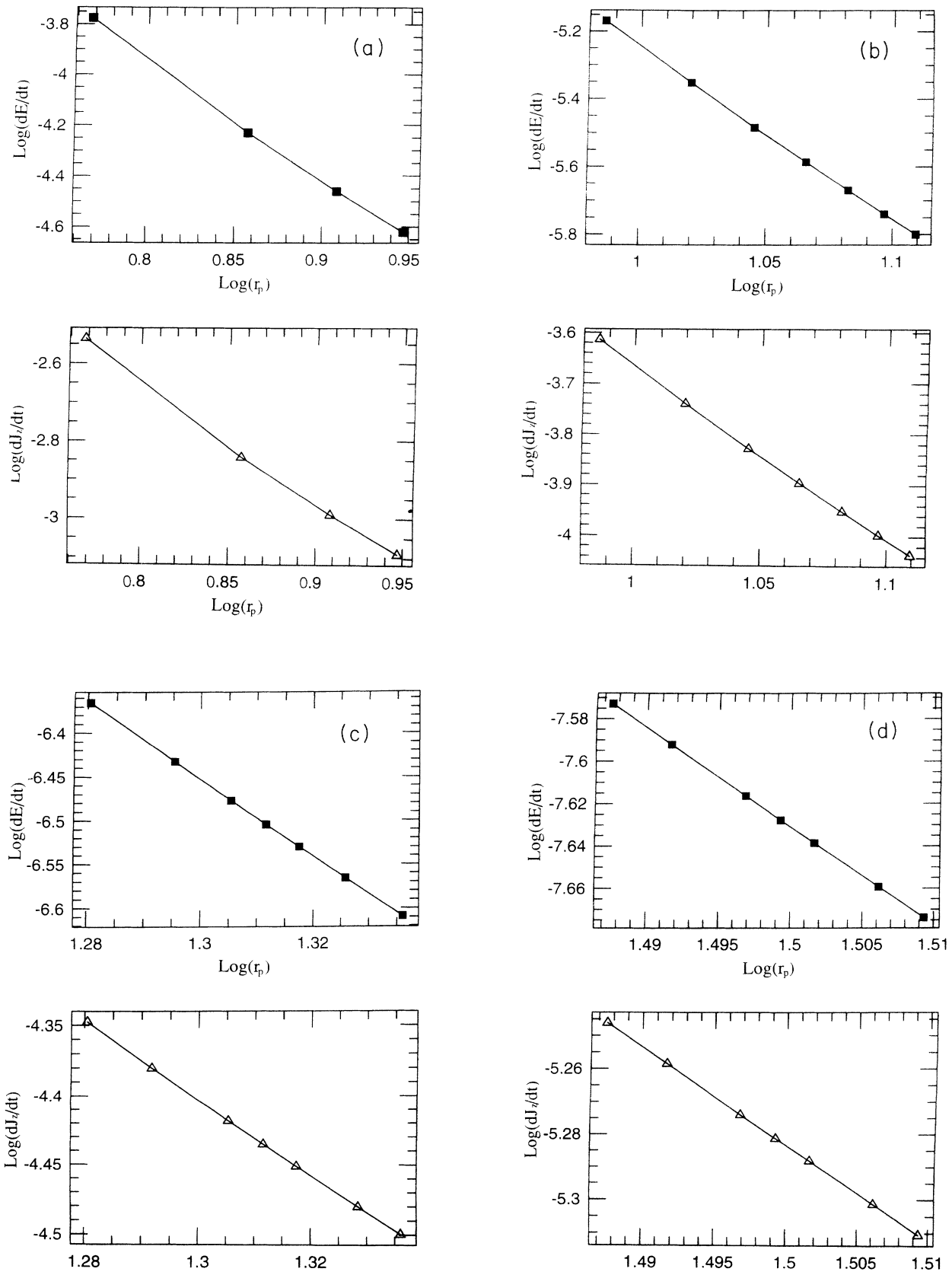

FIG. 5. The energy and angular momentum fluxes for various a, but the same (E', L_z) as a function of $\log(r_p/M)$. In each figure, the filled square and closed triangle denote the energy and angular momentum fluxes, respectively. The adopted parameters are shown in Table I. The logarithm is base 10.

TABLE I. Parameters for Fig. 5. Units of dE/dt and dJ_z/dt are $(\mu/M)^2$ and $M(\mu/M)^2$, respectively.

E'	L_z/M	a/M	dE/dt	dJ_z/dt	r_p/M	r_a/M	Fig. 5
0.9657447163	3.77964473	0	1.6788×10^{-4}	2.9145×10^{-3}	5.86626	20.2660	
		0.3	5.8882×10^{-5}	1.4384×10^{-3}	7.19879	19.9885	(a)
		0.6	3.4611×10^{-5}	1.0238×10^{-3}	8.09872	19.6956	
		0.9	2.3893×10^{-5}	8.1351×10^{-4}	8.84992	19.3848	
0.9859489306	4.850712501	−0.9	6.7888×10^{-6}	2.4349×10^{-4}	9.68526	57.7696	
		−0.6	4.4452×10^{-6}	1.8229×10^{-4}	10.4707	57.6873	
		−0.3	3.2806×10^{-6}	1.4854×10^{-4}	11.0976	57.6054	
		0	2.5922×10^{-6}	1.2702×10^{-4}	11.6274	57.5237	(b)
		0.3	2.1375×10^{-6}	1.1182×10^{-4}	12.0886	57.4424	
		0.6	1.8196×10^{-6}	1.0063×10^{-4}	12.4973	57.3615	
		0.9	1.5864×10^{-6}	9.2055×10^{-5}	12.8636	57.2810	
0.986930827	5.77350269	−0.9	4.3135×10^{-7}	4.4910×10^{-5}	19.0746	54.6667	
		−0.6	3.8314×10^{-7}	4.1664×10^{-5}	19.5786	54.5166	
		−0.2	3.3330×10^{-7}	3.8174×10^{-5}	20.2004	54.3162	
		0	3.1295×10^{-7}	3.6704×10^{-5}	20.4925	54.2160	(c)
		0.2	2.9498×10^{-7}	3.5381×10^{-5}	20.7733	54.1157	
		0.6	2.6475×10^{-7}	3.3099×10^{-5}	21.3040	53.9150	
		0.9	2.4608×10^{-7}	3.1651×10^{-5}	21.6775	53.7646	
0.9932955700	7.29324957	−0.9	2.6738×10^{-8}	5.6733×10^{-6}	30.7298	116.116	
		−0.6	2.5575×10^{-8}	5.5141×10^{-6}	31.0266	116.047	
		−0.2	2.4190×10^{-8}	5.3209×10^{-6}	31.3935	115.956	
		0	2.3564×10^{-8}	5.2327×10^{-6}	31.5710	115.910	(d)
		0.2	2.2983×10^{-8}	5.1506×10^{-6}	31.7434	115.865	
		0.6	2.1913×10^{-8}	4.9967×10^{-6}	32.0735	115.776	
		0.9	2.1192×10^{-8}	4.8920×10^{-6}	32.3086	115.709	

$$h_{xx} = -\frac{2\mu M}{Ra_0(1-e^2)}(\cos 2\varphi + e\cos^3\varphi). \tag{3.16}$$

In this case, the Fourier components appear for $\omega = n\omega_0$, where $\omega_0 = (M/a_0^3)^{1/2}$, and become [19,24]

$$\tilde{h}_{xx}(n) = -\frac{2\mu a_0^2}{R}(n\omega_0)^2\left[\frac{1-e^2}{2}\frac{1}{n}J_n'(ne) - \frac{1}{n^2e^2}J_n(ne)\right]$$
$$= -\frac{2\mu M^{2/3}}{R}\left(\frac{T}{2\pi}\right)^{4/3}(n\omega_0)^2 g_{xx}(e), \tag{3.17}$$

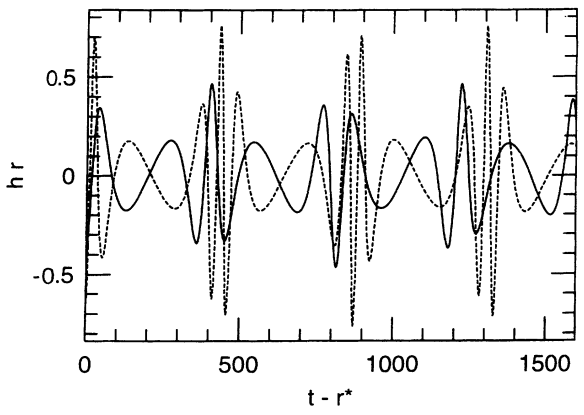

FIG. 6. Waveforms of gravitational waves observed along the spin axis (z axis) for $a = 0$ (dotted line) and $0.9M$ (solid line), and $(E', L_z/M) = (0.9657447163, 3.77964473)$.

where J is the Bessel function. From the same procedure,

$$\tilde{h}_{yy}(n) = -\frac{2\mu M^{2/3}}{R}\left(\frac{T}{2\pi}\right)^{4/3}(n\omega_0)^2 g_{yy}(e). \tag{3.18}$$

Since the following result is essentially the same for the × mode, we only pay attention to the + model seen along the z axis, which becomes

$$\tilde{h}_+ = -\frac{2\mu M^{2/3}}{R}\left(\frac{T}{2\pi}\right)^{4/3}(n\omega_0)^2$$
$$\times\left[\frac{1-e^2}{e}\frac{1}{n}J_n'(ne) - \frac{2-e^2}{2n^2e^2}J_n(ne)\right]. \tag{3.19}$$

We should note that the shape of the Fourier spectrum is completely determined by the eccentricity e. In Fig. 7, we show the Fourier spectrum $|\tilde{h}_+|$ for $e = 0.4, 0.6$ as examples. For orbits with low eccentricities, there appears one peak at $n = 2$ in the Fourier spectrum. This is natural because in the limiting case $e = 0$, all the Fourier components except $n = 2$ disappear. On the other hand, we can see two characteristic angular frequencies for more eccentric orbits; one is ω_0, and another is one determined by the periastron, which is about $(M/r_p^3)^{1/2} = (1-e)^{-3/2}\omega_0$.

Let us consider parameters to be observed from a signal of gravitational waves emitted by a star with a highly eccentric orbit around a SMBH. Provided that an ideal detector (i.e., a detector with a sufficient small noise level)

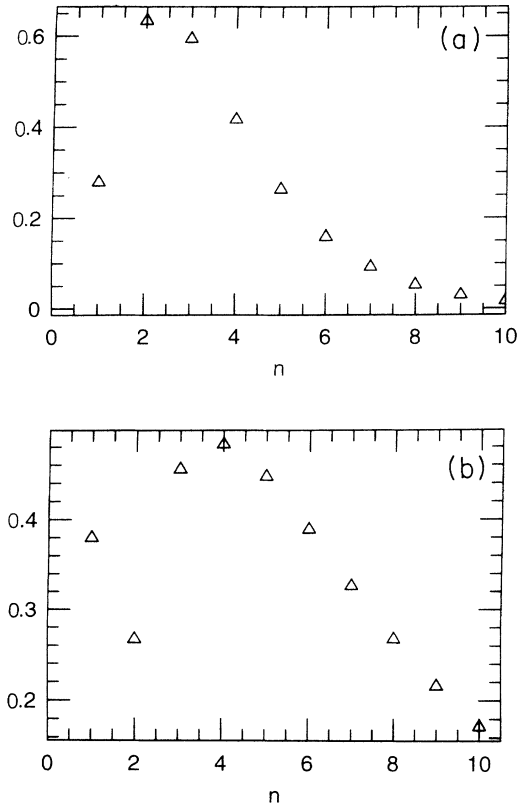

FIG. 7. The Fourier components of gravitational waves (h_+ mode) for eccentric orbits of $e = 0.4$, 0.6 in the Newtonian limit. The horizontal line shows $n = \omega/\omega_0$.

exists, we can extract the following quantities from the Fourier spectrum: the amplitude, the spectrum shape, and the basic angular frequency ω_0. Then we can obtain (1) e from the spectrum shape because it depends only on e; (2) T from ω_0, which can be measured from the frequency of the first peak or from the difference of frequencies between two peaks of the spectrum; and (3) $M^{2/3}\mu/R$ from the amplitude of the spectrum. Once we obtain e and T, we can also know E and L_z of the star. To know the masses M, μ and the distance R, we need additional information. As for the mass of the SMBH, M, it does not seem difficult to obtain: If we extract the first PN effects, we will additionally obtain the ratio M/a_0 because every correction appears as a function of M/a_0 [for example the periastron shift is $6\pi M/a_0(1-e^2)$]. Since $\omega_0 = (M/a_0^3)^{1/2}$, M is obtained from ω_0 and a PN correction term such as the periastron shift. However, we cannot obtain R and μ. It is quite natural because of the equivalence principle, which states that a trajectory of a test particle in an external graviational field is independent of its mass. To obtain μ, we need other information, such as the change rate of the orbital period by the radiation reaction. As for the spin of a SMBH, it seems possible to measure it if we can extract the P$^{3/2}$N effect. This is very similar to the procedure in extracting parameters from the pulse from pulsars [25]. Thus it seems possible to measure parameters for the SMBH as well as orbital parameters of a test particle, (E', L_z) [26].

Next we consider the spectrum for relativistic orbits. From Eq. (3.5), Fourier components of gravitational waves are written as

$$h_+(\omega) - ih_\times(\omega) = \frac{16\pi}{R\Delta t}\sum_l \frac{X_{lm\omega_n}}{c_0}\frac{{}_{-2}S_{lm}^{a\omega_n}}{\sqrt{2\pi}} \times\delta(\omega-\omega_n)e^{i\alpha_{m\omega}}, \quad (3.20)$$

where $\alpha_{m\omega} = \omega r^* - m\varphi$ is a phase factor. $h_+(\omega)$ and $h_-(\omega)$, respectively, become

$$h_+(\omega) = \frac{16\pi}{R\Delta t}\left|\sum_l \frac{X_{lm\omega_n}}{c_0}\frac{{}_{-2}S_{lm}^{a\omega_n}}{\sqrt{2\pi}}\right| \times\delta(\omega-\omega_n)\cos(\alpha_{m\omega}+\eta_{m\omega}), \quad (3.21)$$

$$h_-(\omega) = -\frac{16\pi}{R\Delta t}\left|\sum_l \frac{X_{lm\omega_n}}{c_0} - \frac{{}_{-2}S_{lm}^{a\omega_n}}{\sqrt{2\pi}}\right| \times\delta(\omega-\omega_n)\sin(\alpha_{m\omega}+\eta_{m\omega}),$$

where

$$\tan\eta_{m\omega} = \frac{\mathrm{Im}(\sum_l {}_{-2}S_{lm}^{a\omega_n} X_{lm\omega_n}/c_0)}{\mathrm{Re}(\sum_l {}_{-2}S_{lm}^{a\omega_n} X_{lm\omega_n}/c_0)}.$$

To see the shape of the spectrum with respect to ω, we define the following quantity as a Fourier spectrum:

$$Rh(\omega) = \frac{16\pi}{\Delta t}\left|\sum_l \frac{X_{lm\omega}}{c_0}\frac{{}_{-2}S_{lm}^{a\omega}}{\sqrt{2\pi}}\right|. \quad (3.22)$$

In Figs. 8(a) and 8(b), we show $Rh(\omega)$ for $(E', L_z/M) = (0.97187295, 4.0)$ and $a/M = 0$, 0.9 as examples. In the figures, the open triangle and filled triangle denote the Fourier spectrum of gravitational waves observed along the spin axis and in the direction of $\theta = \pi/4$, respectively. In these cases, $2\pi/\Delta T$ and $\Delta\varphi/\Delta T = \omega_0$ become $0.0115M^{-1}$ and $0.0169M^{-1}$ for $a = 0$ and $0.0118M^{-1}$ and $0.0142\mathrm{M}^{-1}$ for $a = 0.9M$. It is found that the feature of the spectrum shape is similar to the case of the Newtonian orbit: There are two characteristic frequencies, one is $\sim \omega_0$ and another is determined by the motion in the vicinity of the periastron. Details of the spectrum shape are somewhat different from that in the case of the Newtonian orbit. For example, the frequency of the first peak does not correspond to ω_0. For both $a = 0$ and $a = 0.9M$ cases, it corresponds to $(m, n) = (2, -1)$. However, the global shape of the spectrum is essentially the same as that for the Newtonian orbit. Hence, if we prepare accurate theoretical templates, it will be possible to extract parameters of the SMBH as well as orbital parameters of a test particle from a signal of gravitational waves.

The spectrum shape is also different depending on the direction of the observation as found in Figs. 8(a) and 8(b). In the case that an observer detects the signal along the spin axis, he only detects modes of $|m| = 2$ because of the property of the spheroidal harmonics [19]. However,

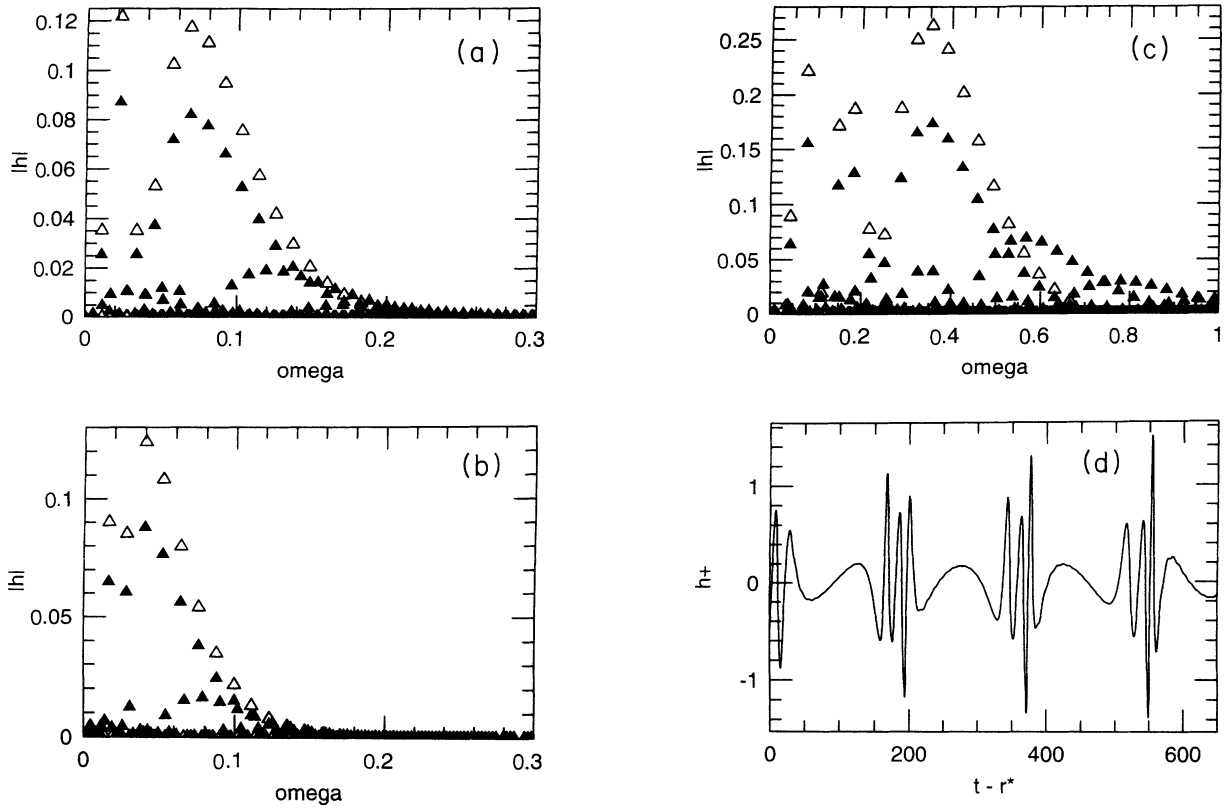

FIG. 8. The Fourier components of gravitational waves $Rh(\omega)$ in the case of general relativistic eccentric orbits, $(E', L_z/M) = (0.97187295, 4.0)$ for (a) $a = 0$ and (b) $a = 0.9M$. The open triangle and filled triangle denote the spectrum of gravitational waves detected along the z axis ($\theta = 0$) and $\theta = \pi/4$, respectively. The unit of the horizontal axis is M^{-1}. The Fourier component $Rh(\omega)$ is shown in (c) and the waveform Rh_+ is shown in (d), each for gravitational waves with $a = 0.9M$ and $(E', L_z/M) = (0.93, 2.5)$. The open triangle and filled triangle denote the spectrum of gravitational waves detected along the z axis ($\theta = 0$) and $\theta = \pi/4$, respectively.

if he observes the signal along the other directions, he will detect modes of $|m| \neq 2$ as well as those of $|m| = 2$. For the highly relativistic orbits, such modes have large amplitudes. In Fig. 8(c), we show the spectrum for $(E', L_z/M) = (0.93, 2.5)$ and $a = 0.9M$ ($r_p = 2.48M$, $2\pi/\Delta T = 0.0346M^{-1}$, $\omega_0 = 0.0739M^{-1}$). In this case, the peak amplitude for $|m| = 3$ is about one third as large as that for $|m| = 2$. In Fig. 8(d), we also show the waveform (+ mode) seen along $\theta = \pi/4$. It is found that the waveform has a very complicated shape because of the relative enhancement by the higher multipole modes. So, we may expect to find such a mode in the shape of the spectrum even in the noisy data. Since the relative strength of the mode of $|m| = 3$ to the mode of $|m| = 2$ also depends on parameters of the SMBH as well as the orbital parameters of a test particle, it will be of some help for us in extracting parameters from a signal.

IV. DISCUSSION

As we show in Sec. III, the quadrupole formula underestimates the energy and angular momentum fluxes of gravitational waves by a large factor; as for the energy flux, the factor for $r_p \sim 10M$ is ~ 2 for $a = 0.9M$, ~ 5 for $a = 0$, and ~ 10 for $a = -0.9M$, respectively. As for the angular momentum flux, the factor is ~ 1.5 for $a = 0.9M$, ~ 2 for $a = 0$, and ~ 3 for $a = -0.9M$. Suppose that the energy and angular momentum fluxes becomes five times and twice as large as those by the quadrupole formula. (This corresponds to the case for $a = 0$). From Eqs. (1.4)–(1.6), we find that even if r_p becomes about $6M$, the sufficient energy to satisfy $t_{\rm GWJ} < t_r$ is dissipated. In this case, the duration time t_d is invariant even if r_p changes; so, from Eq. (1.12), the event rate becomes about $1.5^{7/2} \simeq 4$ times. It is somewhat complicated to estimate the event rate for the spinning SMBH. In the case $a = 0.9M$, the energy and the angular momentum fluxes are, respectively, twice and 1.5 times as large as those by the quadrupole formula. In this case, the allowed value for r_p does not change so much. In the case $a = -0.9M$ (i.e., retograde orbit), the energy and angular momentum fluxes are, respectively, 10 and 3 times as large as those by the quadrupole formula. In this case, r_p may become twice, so that the captured rate for the regrograde orbit seems to become about $2^{7/2} \sim 10$ times larger than that for the prograde orbit. On the other hand, $r_{\rm MB} \sim 2M$ for $a = 0.9M$ and $r_{\rm MB} \sim 7M$

for $a = -0.9M$, so a star with a prograde orbit is not susceptive to plunge into the SMBH, whereas a star with a retrograde orbit is susceptible to plunge. Hence, the event rates for the retrograde and prograde orbits will be almost the same, and they will be considerably higher than that estimated by the quadrupole formula. In any case, the event rate becomes larger than that estimated in Sec. I if we take into account the relativistic effects to the energy and angular momentum fluxes, and about 10 events per year will be expected with 1 Gpc.

In Sec. III C, we consider the possibility of extracting parameters of the star and the SMBH of mass $\sim 10^6 M_\odot$ from a signal of gravitational waves. There, the orbital parameters (E, L_z) of the star are not assumed to change because the evolution time scale of the orbit t_d is much longer than the integration time of the detector ~ 1 yr. In this case, the extraction of all parameters except for μ and R seems possible if we can prepare theoretical templates which are accurate enough. For any orbital parameters and observation directions, it will be possible to prepare the accurate template using the perturbation method. Hence, the parameter extraction from a signal of gravitational waves also will be possible if the orbital evolution of the star can be neglected. (It will be possible even in the case that the orbital plane is not the equatorial plane.) However the above assumption is not correct for a SMBH of mass $\lesssim 10^5 M_\odot$ because the evolution time scale becomes $t_d \lesssim 1$ yr. In this case, we must prepare the theoretical template considering the back reaction of gravitational radiation to the particle. For the case that the particle stays on the equatorial plane, it will be possible. The reason is that the appropriate formula for the energy and angular momentum fluxes can be calculated, and then the orbital evolution may be evaluated by the adiabatic approximation [23], since the evolution time scale by gravitational radiation is much longer than the orbital period except for orbits just before plunging into the SMBH. Here, we should notice that the PN formula is not appropriate for a highly relativistic and highly eccentric orbit, so that we need a general relativistic formula. For that, we should perform a more systematic and wider survey of the energy and angular momentum fluxes.

For the case that the particle does not stay on the equatorial plane (i.e., in the general case), the situation is completely different and the problem becomes much more difficult. The reasons are as follows. (1) We can no longer use the adiabatic approximation because it can be applied to the problems in which the orbit of the test particle has some periodicities. Hence, we must consider the back reaction to the test particle locally in time. (2) We must consider the back reaction of not only the energy and angular momentum, but also of the Carter constant of which we do not know the correct physical meaning [19]. To solve the problem (1), we need the elaboration to construct the robust formalism for the radiation reaction which can be applied to strong field and fast motion [23]. In contrast, the back reaction to the Carter constant itself does not seem a serious problem because it will be solved if the solution to problem (1) is found. As described in a previous paper [19], the Carter constant can be written as

$$C = L_x^2 + L_y^2 + a^2(1 - E^2)\cos^2\theta. \tag{4.1}$$

The change rate of it is

$$\frac{dC}{dt} = L_+\frac{dL_-}{dt} + L_-\frac{dL_+}{dt} + a^2(1-E^2)\frac{d\cos^2\theta}{dt}, \tag{4.2}$$
$$+L_+\frac{dJ_-}{dt} + L_-\frac{dJ_+}{dt} - 2a^2E\frac{dE}{dt}\cos^2\theta,$$

where $L_\pm = L_x \pm iL_y$, and dL_i/dt and dJ_i/dt denote the change rates of the angular momentum due to the orbital precession and the radiation reaction. As mentioned in a previous paper [19], the first line can be neglected if the time scale of the radiation reaction is much longer than the orbital period and precession time scale. Because of the condition $\mu \ll M$, the present situation satisfies the relation for the time scales except for orbits just before plunging. Equation (4.2) thus becomes

$$\frac{dC}{dt} = L_+\frac{dJ_-}{dt} + L_-\frac{dJ_+}{dt} - 2a^2E\frac{dE}{dt}\cos^2\theta. \tag{4.3}$$

Therefore, if we can find an expression for the loss rate of the energy and $\pm$ components of the angular momentum by gravitational radiation locally in time, we can evaluate the back reaction of the Carter constant. Thus, problem (2) is attributable to problem (1). Most urgent is the construction of a formalism for the radiation reaction in a Kerr spacetime.

ACKNOWLEDGMENTS

The author thanks T. Tanaka for discussions and comments on the manuscript. He also thanks K. Thorne for kindly sending a copy of the proposal of the LISA project. Numerical calculations were performed on a YHP 715-50 work station. This work was partly supported by the Japanese Grant-in-Aid for Scientific Research of the Ministry of Education, Science and Culture, No. 04234104 and No. 06740343.

[1] R. D. Blandford, in *300 Years of Gravitation*, edited by S. W. Hawking and W. Israel (Cambridge University Press, Cambridge, England, 1987), and references therein.
[2] K. S. Thorne, in *300 Years of Gravitation* [1].
[3] C. Cutler *et al.*, Phys. Rev. Lett. **70**, 2984 (1993).
[4] K. Danzmann *et al.*, LISA Proposal for a Laser-Interferometric Gravitational Wave Detector in Space (1993).

[5] M. G. Haehnelt, Mon. Not. R. Astron. Soc. **269**, 199 (1994).
[6] T. Nakamura, K. Oohara, and Y. Kojima, Prog. Theor. Phys. Suppl. **90**, 110 (1987), and references therein.
[7] A. P. Lightman and S. L. Shapiro, Astrophsy. J. **211**, 244 (1977).
[8] A. P. Lightman and S. L. Shapiro, Rev. Mod. Phys. **50**, 437 (1978), and references therein.
[9] S. L. Shapiro and S. A. Teukolsky, *Black Holes, White Dwarfs, and Neutron Stars* (New York, Wiley, 1983).
[10] E. S. Phinney, Astrophys. J. **380**, L17 (1991).
[11] L. E. Kidder, C. M. Will, and A. G. Wiseman, Phys. Rev. D **47**, 4183 (1993).
[12] D. V. Galtsov, A. A. Matiukhin, and V. I. Petukhov, Phys. Lett. **77A**, 387 (1980).
[13] L. Blanchet and G. Schäfer, Mon. Not. R. Astron. Soc. **239**, 845 (1989).
[14] T. Damour and N. Deruelle, Ann. Inst. Henri Poincare **43**, 107 (1985).
[15] H. Goldstein, Classical Mechanics (Addison-Wesley, Reading, MA, 1980).
[16] P. C. Peters and J. Mathews, Phys. Rev. **131**, 435 (1963); P. C. Peters, Phys. Rev. **136**, 1224 (1963).
[17] T. Tanaka, M. Shibata, M. Sasaki, H. Tagoshi, and T. Nakamura, Prog. Theor. Phys. **90**, 65 (1993).
[18] M. Shibata, Phys. Rev. D **48**, 663 (1993).
[19] M. Shibata, Prog. Theor. Phys. **90**, 595 (1993).
[20] M. Sasaki and T. Nakamura, Prog. Theor. Phys. **67**, 1788 (1982).
[21] S. A. Teukolsky, Astrophys. J. **185**, 635 (1973).
[22] T. Apostolatos, D. Kennefic, A. Ori, and E. Poisson, Phys. Rev. D **47**, 5376 (1993).
[23] C. Cutler, D. Kennefic, and E. Poisson, Phys. Rev. D **50**, 3816 (1994).
[24] L. Blanchet and G. Schäfer, Class. Quantum. Grav. **10**, 2699 (1993).
[25] For example, J. H. Taylor and J. M. Weisberg, Astrophys. J. **345**, 434 (1989); reference 9, section 16.5.
[26] In the realistic detection of gravitational waves, the frequency of the wave is shifted by the cosmological redshift. Thus, the obtained mass is the so-called redshifted mass [3], and the uncertainty, $\sim 0.3(R/1\ \mathrm{Gpc})$, will appear in determining parameters if we cannot obtain the redshift of the source.